J Mater Sci (2007) 42:3288–3298
DOI 10.1007/s10853-006-0751-y

SIZE-DEPENDENT EFFECTS

Particle size effects in Rh/Al_2O_3 catalysts as viewed from a structural, functional, and reactive perspective: the case of the reactive adsorption of NO

Mark A. Newton · Andrew J. Dent · Steven G. Fiddy · Bhrat Jyoti · John Evans

Received: 1 June 2006 / Accepted: 2 August 2006 / Published online: 22 March 2007

Abstract The structural-dynamic behaviour of γ-Al_2O_3 supported Rh nanoparticles under He, H_2/He, and NO/He has been investigated using a newly developed methodology that permits dispersive EXAFS (EDE), diffuse reflectance infra red spectroscopy (DRIFTS), and mass spectrometry (MS) to be applied simultaneously to the study of gas-solid interactions. This reveals a considerably variability in nanoparticle habit (for 11 Å diameter nanoparticles as a function of temperature), and between 8 Å and 11 Å particles in their response to NO. The selectivity (N_2/(N_2 + N_2O)) of the reactive interaction between NO and the supported Rh shows essentially no particle size dependence above 473 K: it is apparent, however, that considerable differences in some aspects of the structural behaviour of the 8 Å and 11 Å Rh particles do nonetheless, exist. At 373 < T < 473 K a clear divergence in structural, functional, and reactive response of the different sized supported Rh nanoparticles toward NO is observed. These observations are discussed in terms of the ability of different sized Rh particles to change structure in response to the reactive environment, the subsequent effect this has on the nitrosyl functionality that different phases may support, and the reactive pathways for NO conversion that may therefore arise.

M. A. Newton (✉)
The European Synchrotron Radiation Facility,
38043 Grenoble, France
e-mail: newton@esrf.fr

A. J. Dent · J. Evans
Diamond Light Source, Chilton, Oxford, UK

S. G. Fiddy
Synchrotron Radiation Source, Daresbury, Warrington, UK

B. Jyoti · J. Evans
School of Chemistry, University of Southampton, Highfield,
Southampton SO17 1BJ, UK

Introduction

That considerable change in the physical and chemical behaviour of metals and oxides might be expected as their domain size is constrained to below a few tens of angstroms has long been expected and studied [1]. Materials such as catalysts, that are comprised of components residing on these length scales, are required to service ever more wide ranging and specific technological needs. As such the importance attached to a fundamental understanding of how such size dependent effects arise and manifest themselves constantly grows in both academic and industrial arenas.

This research takes many forms and utilises a variety of model approaches. In the current case, that of the behaviour of Rh in deNO_x processes, these range from studies made on flat single crystal Rh surfaces in UHV to Rh particles deposited upon flat oxide surfaces (again predominantly in UHV) [2], though a cornupcopia of high area/elevated pressure studies [3–15]. All of these approaches are to some degree ''models'', involving approximations to various aspects of the ''real'' systems in some way, shape, or form. As such a further question that needs to be asked of all these approaches is in what way, and to what extent, do these implicit approximations—central amongst them for instance being the domain size and dispersion of the

active material—limit their utility in understanding and augmentating the processes under consideration.

The interaction of Rh with NO has for many years been of interest [2–15] as a fundamental step in the global process of the catalytic removal of NO_x gases for pollution control. Infra red spectroscopy has found great utility in such studies, it being sensitive to the surface bound functionality that accompanies, for instance, the interaction and reaction of NO with a catalyst. On its own, however, this spectroscopy is not a direct probe of adsorbate structures or the surface structures that support them, other than through inference.

To this end, and given that many fundamental processes occurring in gas solid interactions can occur very rapidly, we have developed and implemented a new methodology [14, 15] that permits in situ investigation of such interactions using DRIFTS and mass spectrometry along with transmission EXAFS—a spectroscopy that is a direct probe of local structure. By utilising EXAFS in dispersive mode we can interrogate these systems from structural, functional, and reactive viewpoints on a timescale of a few tens of milliseconds. In the current case we use this capacity to investigate how Rh catalysts, with average starting particle diameters in the reduced state of ca. 8 and 11 Å [13–17, 21] respond to NO adsorption between 373 K and 573 K.

Experimental

The work described here was carried out at the dispersive EXAFS beamline of the ESRF (ID24). Dispersive EXAFS measurements were made at the Rh K edge using a Si [311] polychromator mounted in a Bragg configuration and using a 14-bit ADC FReLoN detector [15, 16]. The implementation of the FReLoN detector for dispersive EXAFS studies has largely negated the previous limitation in spectral acquisition rates. Due to CCD readout time previous data collection was limited to, at best ca. 3 spectra per second. The FReLoN permits data acquisition with only 0.8 ms dead time and obtaining up to 500 spectra per second is now possible. Typically, EDE spectra were collected with 62 ms (~17 spectra per second) time resolution. The infrared measurements were made using a Digilab FTS 7000 spectrometer equipped with a narrow band, linearised, MCT detector, with a spectral repetition rate of 64 ms, and with 4-cm^{-1} resolution.

Samples were prepared from a wet impregnation of $RhCl_3$ to γ-Al_2O_3 (AlonC, Degussa) and subjected to previously described calcination and reduction procedures [13–17, 21]. About 30–40 mg of these samples (90–120 μm sieve fraction) were loaded into a custom built cell, based upon a design due to McDougall et al. [18]. This arrangement permits study to ca. 673 K sample temperature. The cell was interfaced to a mass spectrometer (Pfeiffer ''Omnistar'') via a differentially pumped stainless steel capillary. The leak tight nature of the system was verified using the mass 32 signal obtained with the mass spectrometer valved off from the cell as compared to that derived with the system open to the various gas flows. Gases were admitted to the system under mass flow control and switched between the cell and a bypass using 4-port microelectric switching valves (Valco). All gas mixtures were used as supplied (Air Liquide) save for the He for which a further in line combined moisture/O_2 trap (Agilent) was utilised.

Samples were subjected to brief oxidation and reduction under flowing 5%H_2/He and 5%O_2/He at 573 K to remove any adventitiously adsorbed carbon species [15]. The sample temperature was then adjusted to that desired for experimentation. A typical experiment involved switching from an inert (He) to a reactive gas flow (5%NO/He or 5%H_2/He). At the same time EDE/DRIFTS/MS data acquisition was initiated.

Reduction of the dispersive EXAFS data and subsequent analysis was performed using PAXAS [19] and EXCURV [20]. Room temperature Rh foil spectra were also collected to permit energetic calibration of the EDE spectra.

Results

Figure 1 (a) shows k^3 weighted EDE derived from 5-wt% to 2-wt% Rh samples at 373 K and 573 K maintained under flowing H_2/He. Figure 1 (b) shows the equivalent data after exposure of the samples to 5%NO/He for 50 s. Where formal fitting in EXCURV proved reasonable, given the data quality, structural and statistical parameters are given in Table 1.

In all cases, in the presence of H_2, an *fcc* nanoparticulate structure is indicated. Variations in net particle size and Rh–Rh bondlengths are, however, also suggested, as functions of temperature and Rh loading. The apparent variations in first shell Rh–Rh co-ordination numbers (CN) as a function of temperature for each system is shown in Fig. 2.

Below 473 K the net CN of the Rh in the 5 wt% case is as expected from our previous studies (ca 7; ~35–50 atoms) [13–17, 21]. What is somewhat surprising is, that between 473 and 573 K, the average Rh–Rh CN and, in the first approximation, the average particle

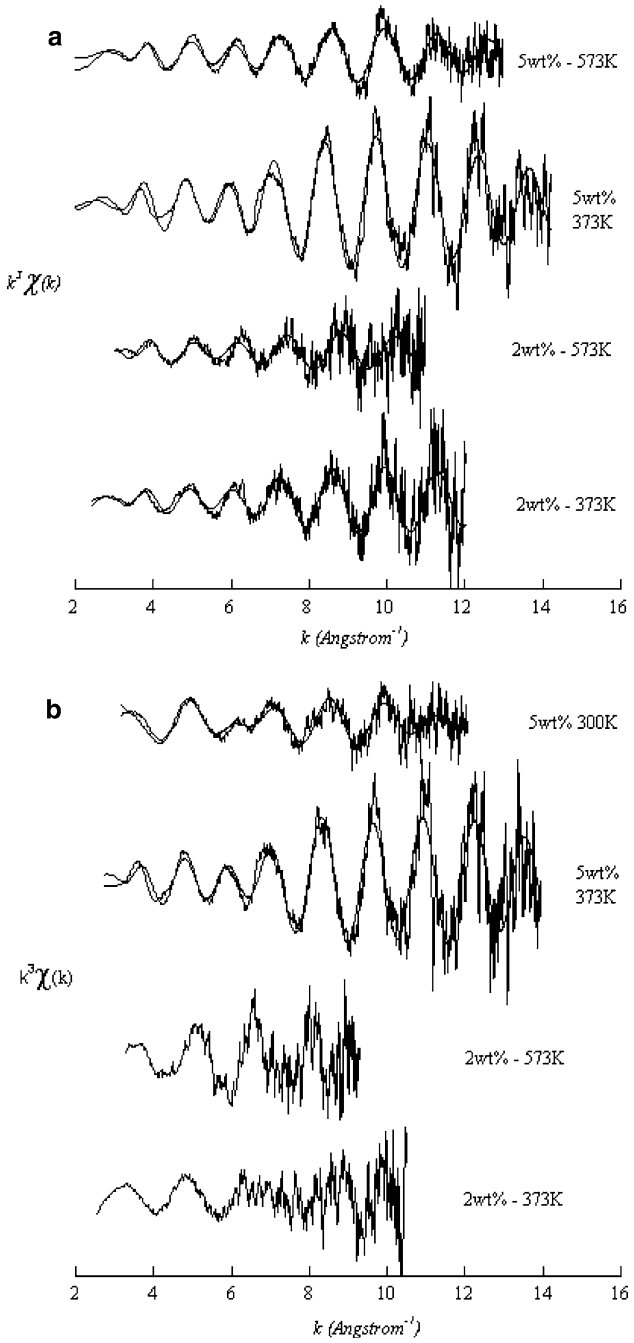

Fig. 1 (**a**) k^3 weighted Rh K edge EXAFS spectra derived from 5 wt% to 2 wt% Rh/Al_2O_3 samples in their reduced state maintained under flowing 5%H_2/He at 373 K and 573 K as indicated. Each spectrum was acquired in 62 ms. Fits from analysis in EXCURV are shown in each case. (**b**) k^3 Weighted Rh K edge EXAFS spectra derived from 5 wt% and 2 wt% Rh/Al_2O_3 after 50 s of exposure to 5%NO/He at 373 K and 573 K as indicated. Each spectrum was acquired in 62 ms. Fits, where deemed reasonable, from formal analysis in EXCURV are shown in each case

size, in the 5-wt% system diminishes considerably. We note that within the temperature range investigated, the variations obtained in Debye Waller (DW) factors as a function of temperature are found to be linear. As such there is no indication that the precipititous drop in apparent Rh–Rh CN in the 5 wt% case is related to effects due to an asymmetric Rh–Rh pair distribution function [22, 23].

Below ca. 550 K the average CN observed in the 2 wt% system is constant at around 4–4.5 (again consistent with previous studies for similar systems [24, 25]) indicating particles of an average atomicity of ca. 10–15 Rh atoms. In this case it is only at 573 K there is any indication of a decrease in CN. As opposed to the apparent variation in CN obtained in the 5 wt% case, however, whether this is can be considered significant, within the error associated with the measurement (between 10% and 20% of the quoted value), is debatable.

After 50 s exposure to 5% NO/He it is only in the 5 wt%Rh-373 K case that the characteristic EXAFS envelope of *fcc* Rh is retained. Even in this case, however, both the amplitudes and the phase of the Rh EXAFS are different to those obtained before NO exposure under 5%H_2/He. These changes indicate that even at 373 K the Rh is significantly perturbed simply through (at this temperature predominantly molecular) NO adsorption. This perturbation is most simply interpreted as a net reduction in the average particle size (or a morphological ''flattening'') of the Rh component in response to NO adsorption. A second possibility is, however, that the smaller particles in the particle size distribution are actively corroded by the NO, whilst the largest resist such a process; it is the latter component that still yields a clear fcc EXAFS envelope. The resulting CN is, however, the average from that obtained from all the Rh species present, many of which may not yield any Rh–Rh-co-ordination at all if they are mono-disperse, isolated Rh atom species.

At 573 K the analysis of the post NO data in the 5-wt% case clearly indicates the formation of an oxidic form of Rh. At the same time, however, it is clear that this phase is distinct from that formed through exposure to O_2 or air alone. This is most clearly evidence in the XANES where the intensity of the white line is significantly diminished and of a differing shape relative to that obtained on the latter case [21, 26].

In the 2-wt% cases the data obtained post NO exposure is somewhat truncated and not considered formally fittable (and as such no fits are shown). Nonetheless, it is clear that no vestige of what would be expected from an *fcc* Rh system remains even at 373 K. Indeed the evidence would suggest that at even 373 K, and in stark contrast to the 5 wt% system, the adsorption of NO has completely changed the phase of

Table 1 Structural and statistical parameters derived from the dispersive EXAFS spectra shown in Fig. 1 after reduction using PAXAS and [19] analysis using EXCURV [20]

Sample	T (K)	Gas (5% in He)	k_{min} (Å^{-1})	k_{max} (Å^{-1})	Scatterer	CN	R (Å^{-1})	DW ($2\sigma^2$)	E_F (eV)	R (%)
5 wt%	373	H_2	2	14,00	Rh	6,8	2,67	0,012	3,20	48
5 wt%	573	H_2	2	13,00	Rh	5,1	2,64	0,016	0,60	44
2 wt%	373	H_2	2	12,00	Rh	4.0	2,62	0,014	–0,50	64
2 wt%	573	H_2	3	11,00	Rh	3.3	2,62	0,020	1,24	73
5 wt%	373	NO	3	14,00	Rh	3,8	2,70	0,009	–3,62	51
5 wt%	573	NO	3	12,00	Rh	1,7	2,65	0,015	1,94	52
					O	1,9	2,06	0,01		
					N	0,8	1,88	0,009		

Spectral acquisition times in each case were ca. 65 ms

Errors in CN should be considered in the range ±10–20%, those of bondlengths (r) ± 1.5–2%

$R(\%) = (\int [\chi^T - \chi^E] k^3 dk / [\chi^E] k^3 dk) \times 100\%$: χ^T being the theoretically calculated EXAFS and χ^E being the EXAFS obtained via experiment

σ = the root mean square displacement in internuclear separation

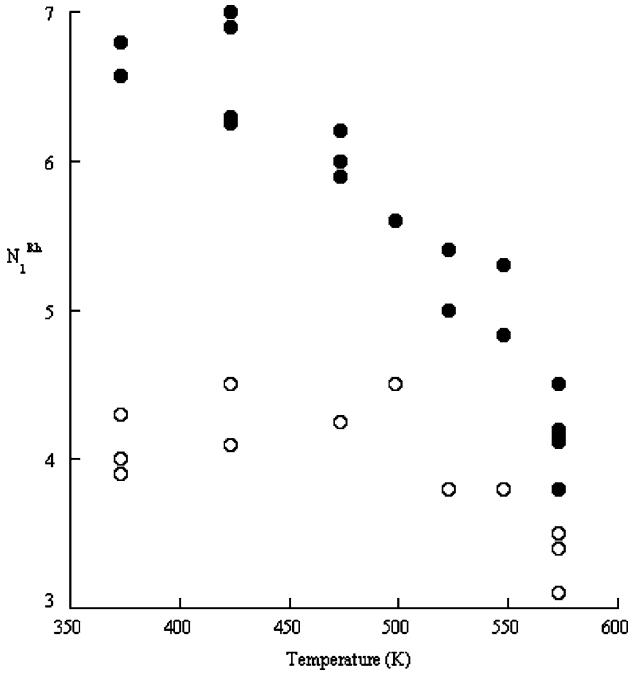

Fig. 2 Variation in fitted first shell Rh–Rh co-ordination number (CN) as a function of sample temperature for 2 wt% and 5 wt% Rh/Al_2O_3 samples maintained under flowing H_2/He. CN's derived from formal analysis using EXCURV. Errors in CN determination should be regarded as being in the range of ±10–20% of the quoted values

the Rh, much as CO has widely been shown to oxidatively disrupt Rh particles of a similar size to yield supported $Rh^I(CO)_2$ species [21, 24, 25, 27].

Figure 3a and b show the DRIFTS spectra obtained after 50 s exposure of the Rh samples to 5%NO/He at either end of the temperature range investigated. At 573 K the DRIFTS spectra obtained in each case are very similar. In both cases the spectra are dominated by absorption at ca. 1911 cm^{-1} associable with a linear $(NO)^+$ species, [4–9] though residual contributions present at lower (ca. 1640 cm^{-1} and 1740 cm^{-1}) wavenumber persist. Upon the removal of NO, and replacement with He, it is only the linear NO^+ species that is stable at this temperature.

At 373 K a more diverse array of nitrosyl functionality is observed in each case and some significant differences can now be observed between the two systems under study. Whilst present in both cases, the NO^+ species is relegated to a minority species. In both cases this is outweighed in intensity by clearly defined bands at 1825 cm^{-1} and 1745 cm^{-1}. These latter bands are indicative of the presence of $Rh(NO)_2$ species [5] and (in the case of the 1745 cm^{-1} band) ''high wavenumber'' $Rh(NO)^-$[2–9]. In at least one case EXAFS has previously shown a species of the latter type to be an isolated, mono-disperse, Rh centre [28].

In the 5-wt% case the most intense band is observed at 1680 cm^{-1}; in contrast this band is virtually absent on the 2-wt% catalyst. In these systems bands between 1500 cm^{-1} and 1700 cm^{-1} can arise from a range of species such as nitrates [4–9], so called ''low wavenumber'' $Rh(NO)^-$ species [4–9] and molecular NO adsorbed upon low index Rh surfaces [10, 11].

Figure 4 again shows IR spectra derived from the 2-wt% system at 373 K. In this case the spectra obtained under NO/He after 50 s exposure (A), is compared to that derived from removing the NO and replacing it with a flow of He (B). Spectrum (C) shows the difference between these two cases. Of most note here is that the removal of the He precipitates a loss of functionality (positive bands) at 1825 cm^{-1} and a broad loss of IR intensity between ca. 1700 cm^{-1} and 1800 cm^{-1}. Concomitantly, a negative (formation) band in the difference at ca. 1930 cm^{-1} is observed.

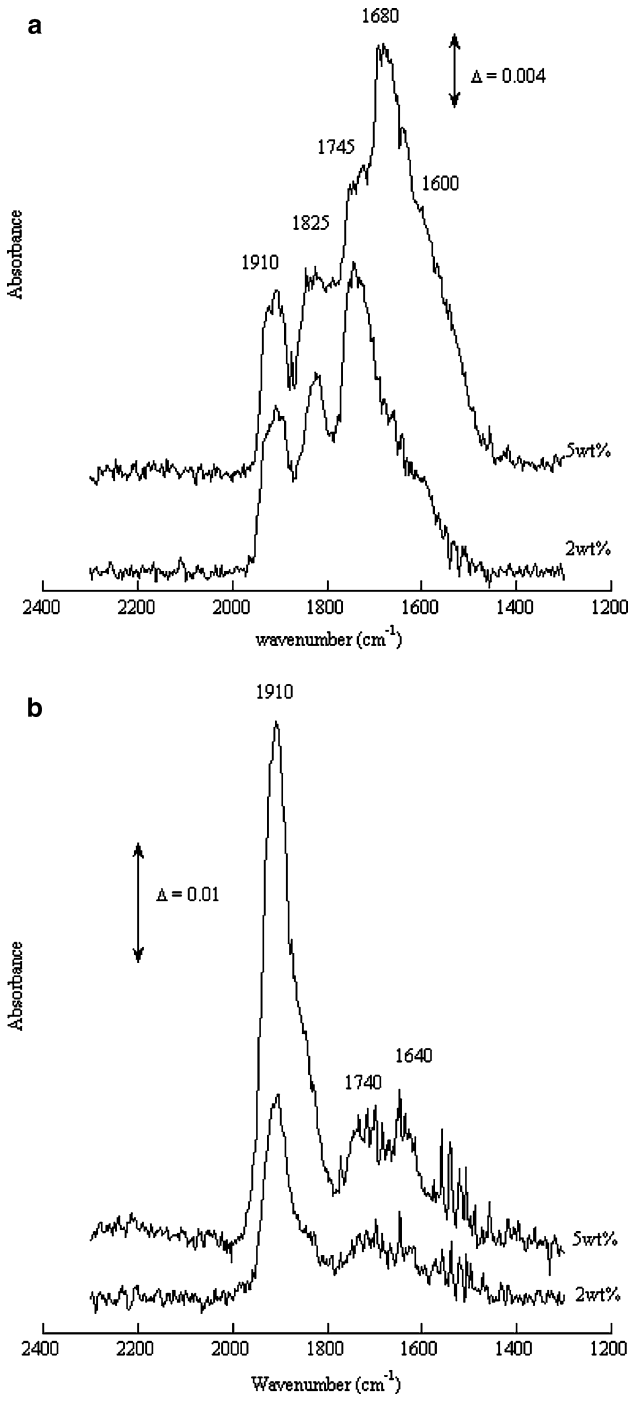

Fig. 3 (**a**) DRIFTS spectra obtained (under flowing 5%NO/He) from 2 wt% and 5 wt% Rh/Al_2O_3 samples after 50 s exposure to 5%NO/He at 373 K. Spectra acquired in 64 ms. (**b**) DRIFTS spectra obtained (under flowing 5%NO/He) from 2 wt% and 5 wt% Rh/Al_2O_3 samples after 50 s exposure to 5%NO/He at 573 K. Spectra acquired in 64 ms

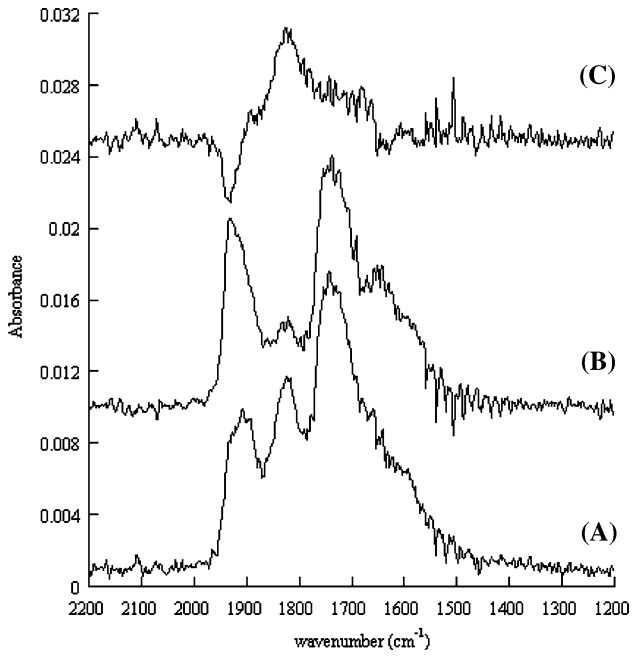

Fig. 4 The effect of replacing flowing 5%NO/He with flowing He on IR spectra derived from 2 wt% Rh/Al_2O_3 at 373 K: (**a**) under flowing 5%NO/He; (**b**) after switching to flowing He; (**c**) the difference between A and B. In spectrum (**c**) a positive band indicates the removal of a species (e.g. ca. 1830 cm^{-1}), a negative band the formation of new species (e.g. 1933 cm^{-1})

Whilst, in this region of the spectrum, interference from bands due to $NO_{(g)}$ is expected, the disappearance of functionality at 1745 cm^{-1} and 1825 cm^{-1}, at the same time as subsequent augmentation of absorbance at around 1930 cm^{-1} is indicative of the following reaction;

$$Rh(NO)_2 \rightarrow Rh(NO)^+ + NO_{(g)} \quad (1)$$

As first observed by Liang et al. [5] and proposed in tandem with a unimolecular decompsition pathway yielding N_2O.

$$Rh(NO)_2 \rightarrow Rh(O) + N_2O_{(g)} \quad (2)$$

Figure 5a and b shows net NO uptake (expressed at NO molecules/Rh atom) and the net selectivity toward N_2 obtained during the interaction of the Rh samples during 50 s exposure to flowing $5\%NO/H_2$. It is clear that, above 473 K, the response of the Rh to NO is essentially the same in both 2-wt% and 5-wt% cases. Below 473 K, however, pronounced differences appear in both net NO uptake and the selectivity of the interaction; the 2 wt% system shows the inverse behaviour to that observed at 5 wt% in terms of both uptake and selectivity. Though in both cases the reactive turnover is low at 373 K, that which does occur strongly favours N_2O in the 2-wt% case.

Figure 6 shows the dynamic response of the two systems to the adsorption of NO as a function of temperature and as measured by changes in Rh K edge

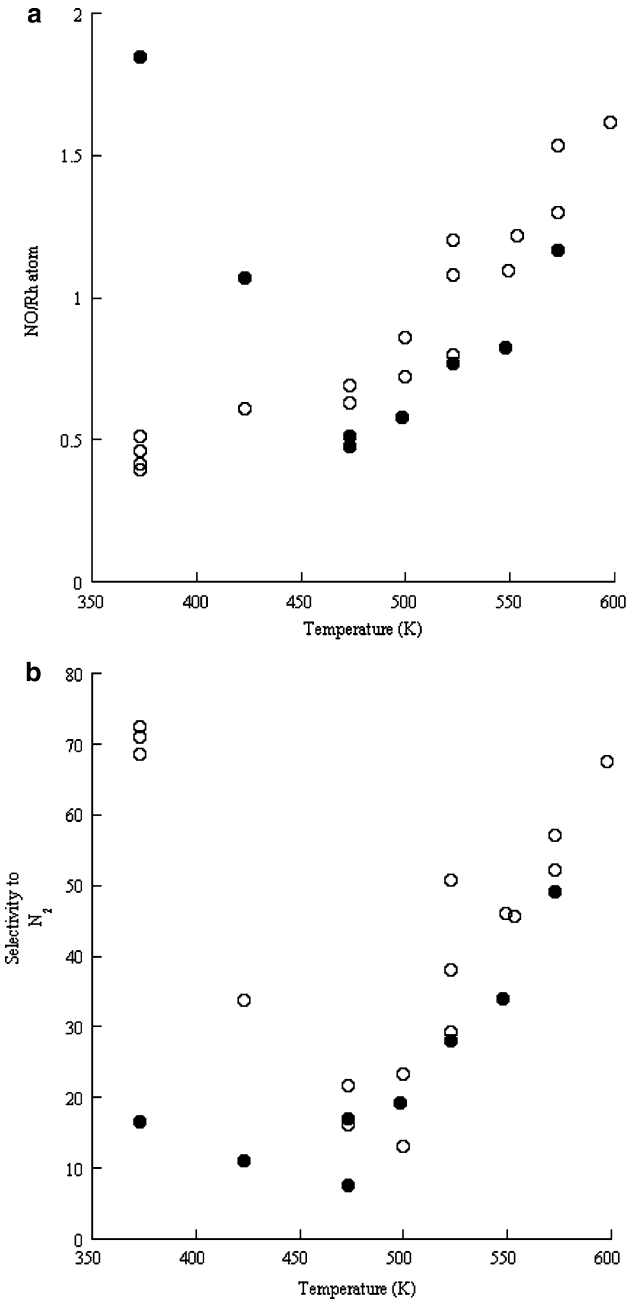

Fig. 5 (**a**) Mass spectrometry derived variation of the net uptake of NO observed to occur during 50 s of 5%NO/He exposure to 5 wt% (open circles) and 2 wt% (filled circles) Rh samples as a function of sample temperature. (**b**) Mass spectrometry derived variation of the net selectivity ($N_2/(N_2 + N_2O)$) toward N_2 achieved during occur during 50 s of 5%NO/He exposure to 5 wt% (open circles) and 2 wt% (filled circles) Rh samples as a function of sample temperature

XANES observed at 23250 and 23270 eV. Each trace has been set to 0 at the beginning of the experiment and as such these plots only those changes due to the interaction of the NO with the Rh.

In the 5 wt% case these data, allied to formal analysis of the EXAFS (not shown), indicate a relatively simple and progressive increase in the degree of oxidation of the Rh phase as a function of temperature, much as we have previously delineated for the oxidation of 5-wt%Rh/Alumina systems such as these using O_2 [16] i.e. a logarithimic rate law, [29, 30] is indicated. Analysis of the initial rates of oxidation leads to the Arrhenius plot shown in Fig. 7 and indicates that the apparent activation energy for this process, in the limit of 0 oxidation, is ca. $E_a \sim 10$–12 kJmol^{-1} and, as such, essentially the same as when O_2 is utilised as the oxidant.

The story revealed by the 2 wt% case using the same type of XANES analysis is, however, rather different. Whilst at $T < 473$ K the overall temporal dependence of the changes in XANES observed are similar to that observed in the 5-wt% case, the behaviour of the system apparently changes radically at 473 K: the magnitude of the apparent changes in XANES structure are suddenly diminished. Clearly above 473 K the 2 wt% is behaving in a very different manner to the 5 wt% system. Yet, both the net selectivity of the interaction and, at least at 573 K, the DRIFTS obtained after 50 s NO exposure, indicate that the predominant nitrosyl formed is the same in both cases. The predominant cause of this observation lies in a rather unexpected ramification of purging the system with flowing He in between making reactive measurements.

Figure 8 shows a comparison of normalised Rh K edge EDE, obtained from 2 wt% and 5 wt% samples at 473 K maintained under flowing 5%H_2/He, and the first spectrum obtained during a switch from flowing He to 5%NO/He i.e. before the switch has occurred. It is abundantly clear that the spectrum obtained under He is rather different to that derived under 5%H_2/He; the systems are not starting from the same point in terms of the Rh phase present in the sample. In the 5% case there is precious little evidence for such a radical change in structure even at 573 K [15].

In the 2 wt% system evidence for this change of phase can be seen even at 373 K, though the extent of the change is attenuated. By 473 K, a switch to He results in this phase change completely before NO exposure can be made. What is clear from this observation is that a direct comparison of the structural-kinetic behaviour of the interaction of NO with reduced 2 wt% Rh nanoparticles (ca. 8 Å diameter), with that of the reduced particles in the 5 wt% case (ca. 11 Å diameter), is not possible using this experimental methodology.

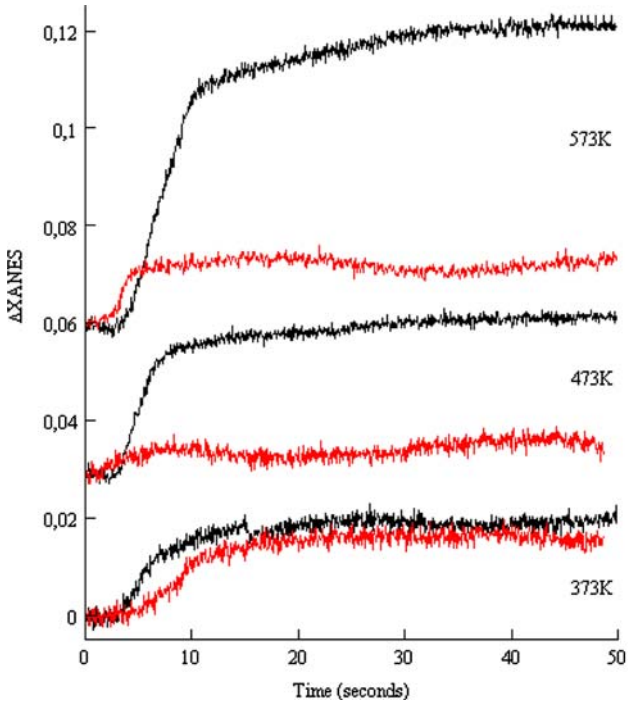

Fig. 6 Temporal variation in Rh K edge XANES observed during exposure of reduced 2-wt% (red) and 5-wt% (black) Rh/Al_2O_3 samples to flowing 5%NO/He at the temperatures indicated

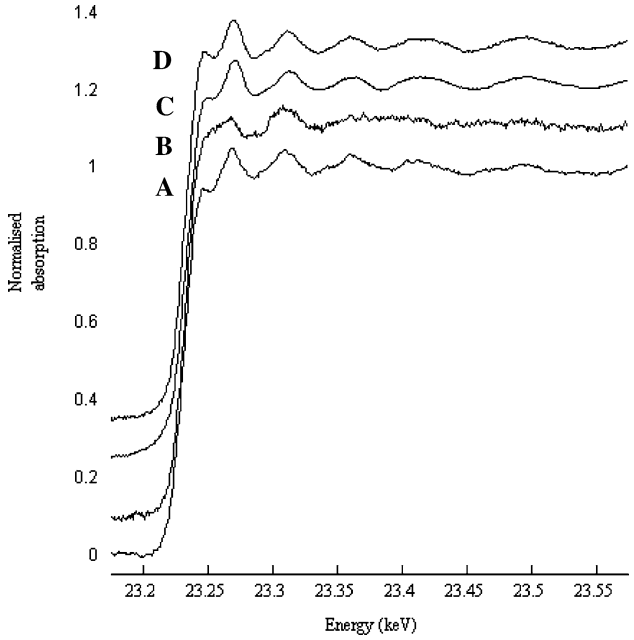

Fig. 8 Normalised Rh K edge EDE spectra derived, at 473 K, from 2 wt% to 5 wt% Rh/Al_2O_3 samples: (**a**) 2 wt% Rh/Al_2O_3 under flowing H_2/He; (**b**) 2 wt% Rh/Al_2O_3 after removal of the flowing H_2/He and replacement with flowing He; (**c**) 5 wt% Rh/Al_2O_3 under flowing He; (**d**) 2 wt% Rh/Al_2O_3 under flowing H_2/He

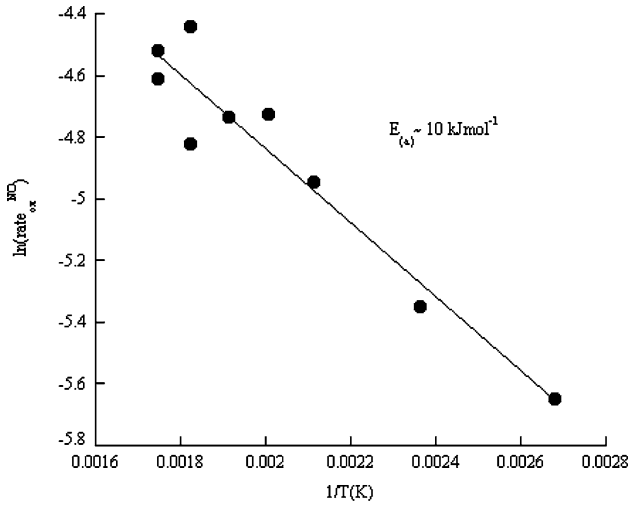

Fig. 7 Arrhenius plot derived from the initial variation (Rh oxidation) of Rh XANES for 5wt% Rh/Al_2O_3 samples

Figure 9 shows the appearance of the $RhNO^+$ functionality in DRIFTS at 3 temperatures. For the reaction of 5 wt% and 2 wt% samples. In each case the intensity of the IR bands has been normalised to 1 at 50 s. At low temperatures the appearance of the $Rh(NO)^+$ species proceeds at a tangibly slower rate on the 5% system than in the 2 wt% case. By 573 K it is clear that the temporal evolution of this species is, in both cases, equivalent.

Figure 10 shows Arrenhius plots derived from the (unnormalised) temporal behaviour of this species for the 2-wt% and 5-wt% cases over the temperature range investigated. What is clear from both of these plots is that, though each case appears to be starting from a significantly different structural points above 473 K, in terms of its normalised rate of appearance during NO exposure, and the apparent activation energy for the formation of the $RhNO^+$ (ca. 17.5–20 $kJmol^{-1}$) their reactive behaviour is essentially the same.

Figure 11 shows the temporal variation of the ratio of IR bands observed at 1745 and 1825 cm^{-1} during the exposure of 2-wt% and 5-wt% samples (as indicated) to NO at 373 K. Also shown are the normalised temporal responses of masses 28 (N_2 and N_2O) and mass 44 (N_2O) during this process.

Again, in terms of these two IR bands, there is a pronounced difference between the two systems under study in their temporal behaviour during NO exposure. In the 5 wt% case this ratio appears essentially invariant (at ca. 0.5) during the experiment and is apparently unrelated to the subsequent formation of the low levels of N_2 that are produced at this temperature.

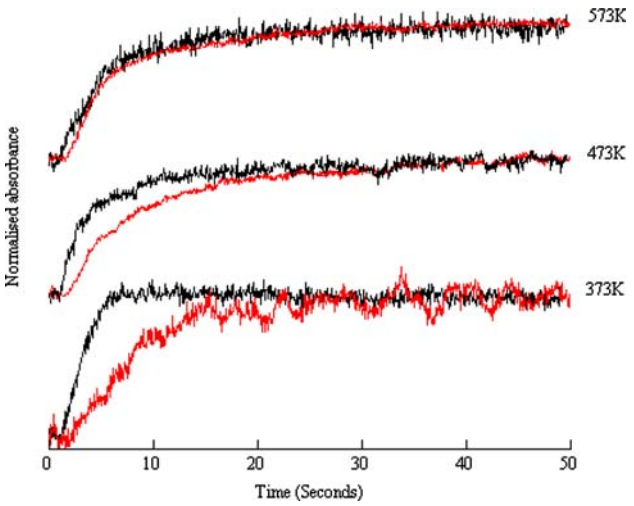

Fig. 9 Temporal variation in the IR absorption at 1911 cm^{-1} during the exposure of 2-wt% (black lines) Rh/Al_2O_3, and 5 wt% (red lines) Rh/Al_2O_3 samples to flowing 5%NO/He at the temperatures indicated. Spectra have been normalised to 1 at $T = 50$ s

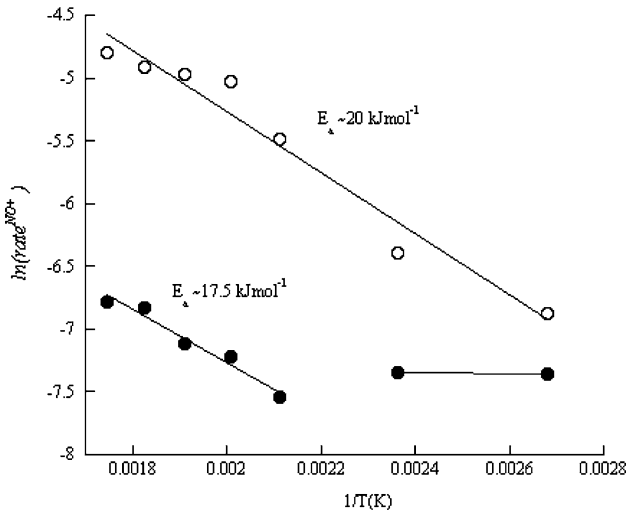

Fig. 10 Arrhenius plots derived from the initial rates of appearance of the IR absorption at 1911 cm^{-1} on 5 wt% (open circles) Rh/Al_2O_3 and 2 wt% (filled circles) Rh/Al_2O_3 during exposure to flowing 5%NO/He

In the 2-wt% case, however, whilst an invariance in ratio is observed after ca. 10 s of NO exposure, the 1745/1825 cm^{-1} ratio is higher (1.5); this period of the interaction is associable with the production of N_2O. The initial value of this ratio in the 2-wt% case is, however, higher still (2.5–3), but rapidly decreases. This inital decrease in 1745/1825-cm^{-1} ratio can be clearly seen to coincide with a short burst of N_2 production in the first 10 s of the experiment over the 2 wt% system.

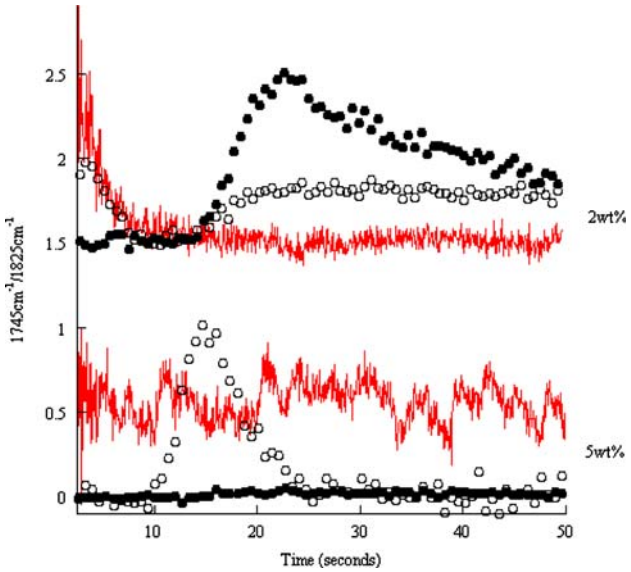

Fig. 11 Comparison of the temporal changes in the ratio of IR absorption at 1745 cm^{-1} and 1825 cm^{-1} (solid lines) observed at 373 K during exposure of Rh/Al_2O_3 samples (as indicated) to flowing 5%NO/He with the evolution of masses 28 (open circles) and 44 (closed circles) in mass spectrometry

$Rh(NO)_2$ species generable in Rh/Al_2O_3 systems of this type have been previously characterised using transmission IR [5]. About 1745-cm^{-1} and 1825-cm^{-1} absorption are expected from this species in ca. 3:1 ratio. It is also the case, however, that contributions due to gas phase NO(g) are also to be expected at 1833 cm^{-1} in our experiment. If we make the assumption that in the 5-wt% case the ratio we observe is essentially that due to these latter gas phase contributions then the real 1745/1825 cm^{-1} ratio we observe after 10 s NO exposure in the 2 wt% system is much closer to 3 (see also spectrum (B), Fig. 4) and therefore that which we might expect from the predominant formation of the $Rh(NO)_2$ species. The increase in ratio observed at $T < 10$ s therefore indicates that a further species is initially evolved during the interaction with NO; a species that only shows a contribution to the IR spectrum at 1745 cm^{-1} i.e. the so called ''high wavenumber'' $Rh(NO)^-$ species [4–9, 28].

Discussion

DRIFTS, dispersive EXAFS, and mass spectrometry can be combined to yield a single experiment capable of addressing the structural, functional, and reactive behaviour in solid or gas-solid systems with high time resolution and at temperatures up to ca 673 K. This approach has allowed us to dissect the interaction of

NO with alumina supported rhodium nanoparticles (with diameters of 8–11 Å in their reduced state), and to reveal an intriguing array of both reactive, structural and functional behaviour within this notionally simple and fundamental interaction.

Mass spectrometrically, the interaction of NO with the two differently sized Rh nanoparticulate systems is essentially identical (in terms of NO turnover per Rh/atom and the net selectivity achieved toward N_2) in the range $473 < T < 573$ K. Similarly, the predominant functionality observed in each case in this temperature range, the linear Rh nitrosyl species, does not indicate any significant size dependent effects.

Yet it is clear from the EXAFS taken during the experiments that, in this temperature range, the Rh starts from significantly differing states in the two cases: in the 5-wt% case progressively smaller, but nonetheless, still fcc Rh nanoparticles; in the 2-wt% case, a new, and as yet structurally unspecified phase, that does not show any of the EXAFS structure expected from reduced Rh nanoparticles. At the same time, however, this phase does not have the XANES structure (a pronounced and intense which line for example) to clearly indicate significant oxidation to, for example Rh 3+ [21, 26].

This structural variation does not, in this instance, appear to have a significant effect on the observed reactivity of the system. At $T > 473$ K in the 5% case reactive oxidation of the Rh dictates the observed chemistry of the system and it would appear that the apparent change in phase that occur in the 2 wt% upon the removal of H_2 from the system (and its replacement with He) does nothing to change the nature of the nitrosyl functionality that may be supported on the catalyst surface. As such the net reactive chemistry remains the same even to the level of the apparent activation energy associated with the formation of the linear Rh nitrosyl species between 473 K and 573 K in both 5 wt% and 2 wt% cases.

But what of the source of this apparent change in structure at 2 wt%? Though variety of structural changes of Rh on and into Al_2O_3 has been postulated and observed, these have only generally been done so at considerably more extreme conditions of temperature and reactive environment [31–38]. Equally, however, and despite the considerable safeguards that we have taken to guard against it, we cannot rule out that this observation is an experimental artefact due to an extreme sensitivity of the reduced Rh nanoparticles to, for instance, O_2, moisture, or support hydroxylation, present at very low levels, and to which the larger 5 wt% Rh particles are kinetically resistant. Whatever the real source of this effect, this example demonstrates in an extremely clear fashion the potential hazards associated with trying to make comparative measurements of the behaviour of supported metallic nanoparticles of this size and reactivity. It also illustrates the value of a multifunctional approach using at least one directly structure sensitive probe (in this case EXAFS); *neither IR or mass spectrometry yield any indication that this structural difference between systems exists at all.*

Size dependent effects that do have a significant effect on performance variables such as the selectivity do, however, appear in these systems once the temperature of the interaction with NO is reduced to below 473 K. In this temperature regime the structural data in the 5 wt% system shows that significant oxidation of the Rh nanoparticles is curtailed and replaced by predominantly molecular NO adsorption. Whilst in the 5% case the net NO uptake reaches a minimum (at ca. 0.4–0.5) NO/Rh, the uptake in the 2-wt% system increases to ca. 1.8 NO/Rh atom over the duration of the experiment. Concurrently the selectivity to N_2 formation in the latter case plummets whereas in the former it remains high.

Here the EXAFS, taken in tandem with the IR and mass spectrometry, shows how this happens. At the 5-wt% loading, and a starting nanoparticle diameter of ca. 11 Å, though it is clear that the particles react structurally to the adsorption of NO, they largely resist oxidative disruption and retain their inherent fcc structure. Whether this is achieved through a global rearrangement of all the Rh to accommodate the largely molecularly adsorbed NO species supported upon smaller/flatter fcc particles, or is the result of a size dependent phase separation (oxidative degradation removing the smaller end of the originally present particle size distribution but leaving the largest intact) is a matter of debate when considered only from the EXAFS point of view.

The IR indicates the predominant formation of reactively inert molecular NO (analogous to those observed on, for instance Rh (111) [10]) adsorbed upon these species with IR absorption at 1680 cm^{-1}. Alongside this the data shown in Figures 3 and 11 indicates that this is accompanied by formation of $Rh(NO)^-$ at 1745 cm^{-1} but probably not significant levels of $Rh(NO)_2$. Similarly the net uptake achieved in the system as measured by MS (0.4–0.4 NO/Rh) would appear to be somewhat on the low side of that which one might expect if significant oxidative disruption was the predominant cause of the apparent changes in EXAFS CN. These two observations would tend to favour the notion of a global rearrangement of all the Rh into smaller/flatter particles covered in molecular NO.

One can also estimate that in order to yield a CN of around 4 from a starting point of ca. 7, using the assumption that all the NO dispersed Rh forms species that do not have a Rh–Rh co-ordination sphere then around 50–60% of the Rh in the system would have to have been oxidatively corroded away to form species such as of $Rh(NO)^-$ and $Rh(NO)_2$. At the very least this would require a net uptake of > 0.5NO/Rh whilst not even counting the NO uptake that must be required to explain the absorption at 1680 cm^{-1}. On balance therefore the evidence provided from the three techniques would suggest that, though some oxidative disruption may be occurring, is not the predominant mode of structural reorganisation at work in the 5-wt% case.

By contrast, in the 2-wt% case, it is clear that any vestige of *fcc* structure that may well have existed beforehand under H_2 is effectively removed rapidly (even at 373 K) and replaced with XAFS indicative of co-ordination of the Rh to low Z atoms (O or N). Though not, in the current instance, structurally definitive, when taken in tandem with the NO uptake data and the IR, these measurements fingerprint particle disruption by NO and the predominant (though not exclusive) formation of isolated $Rh(NO)_2$ species: an uptake of 1.8NO/Rh atom would indicate the formation of these species to the ca. 80% level (assuming that any other nitrosyl species are associated with 1NO/Rh atom or less). Further, the temporal behaviour for the ratio of absorptions at 1745 cm^{-1} and 1825 cm^{-1}, when considered with the evolution of N_2 and N_2O, show that some of this majority $Rh(NO)_2$ species is slowly turned over to yield N_2O. By contrast the ''high wave number $Rh(NO)^-$ species'' also initially formed during this interaction (and not having a spectroscopic component at 1825 cm^{-1}) is turned over to yield a transient burst of N_2.

At higher temperatures, where Rh oxidation by NO dissociation starts to dominate, these differences disappear, presumably as the chemistry is rapidly dominated by oxidic Rh surface behaviour which is domain size independent and does not permit the significant formation of species such as $Rh(NO)_2$. Indeed, the increasingly rapid formation of oxidised Rh at higher temperatures will result in an increased preference for the formation of the, thermally stable, linear Rh nitrosyl species. This species may form directly on the oxidised sites once they are formed. However, it is equally the case that they may form via a transient formation of $Rh(NO)_2$ (see Eq. (1) and Fig. 4).

As such, increasingly fast oxidation at elevated temperature can provide a competitive, and, in the first instance N_2O free, conduit to the removal of the geminal dinitrosyl species as and when they might be formed; even if they are formed to in the 2 wt% system initially, their formation need not lead to high levels of N_2O at elevated temperatures, and no particle size dependence in the selectivity of the interaction with NO need therefore arise.

Conclusions

We have shown, using a new and internally consistent methodology that fuses time resolving probes of structure, reactivity, and functionality, that the structural-reactive behaviour of small Rh particles supported upon γ-Al_2O_3 changes dramatically in the regime 8 Å < diameter < 11 Å at temperatures < 473 K.

At some point between these limits Rh nanoparticles become unstable in the presence of NO and are rapidly disrupted to yield majority (ca. 80%), monodisperse $Rh(NO)_2$, together with bent, ''high wavenumber'', $Rh(NO)^-$ species. As has been suggested before [5, 8, 9], a facile route to N_2O production, even at this low temperature, may therefore arise through the formation of the former species; the latter clearly being associable with the formation of N_2.

At the upper end of this size range the Rh particles appear resist this disruption (at 373 K) but do not remain unaltered by the adsorption of NO. The combined evidence suggests they rearrange to yield smaller/flatter particles covered in molecularly adsorbed NO; some oxidative disruption cannot be ruled out but its role appears minor, and significant amounts of $Rh(NO)_2$ are not formed. In this case the high selectivity to N_2 arising from the low level of reactive chemistry in the 5-wt% case is (again) deduced to arise from the decomposition of bent ''high wavenumber'' $Rh(NO)^-$ species.

Any particle size dependence in the net selectivity of the interaction with NO disappears with increasing temperatures due to the increasing kinetic domination of Rh oxidation. This strongly favours the formation of linear Rh nitrosyl species and, as such, may arrest N_2O formation from any $Rh(NO)_2$ species transiently formed through promoting (Eq. 1) at the expense of unimolecular decomposition (Eq. 2).

Additionally our results appear to have revealed a structural instability in the case of the 2-wt% Rh/Al_2O_3 system which is absent in the 5-wt% case i.e. a clearly definable nanoparticulate fcc Rh structure only exists in the presence of 5%H_2/He in the former system. Removal of the H_2 component above 373 K appears to

precipitate a structural reorganisation of the Rh in the 2-wt% system. At present however, the precise nature of this reorganisation cannot be further specified.

Our results show that the structural behaviour intrinsic to Rh nanoparticles in this size range is highly variable and a complex function of experimental parameterisation. In this particular instance it would seem quite that clear that the transferral of conclusions regarding the reactive behaviour of Rh nanoparticle or surfaces of significantly lower dispersion than studied here, with species such as NO, and perhaps even with temperature itself, is fraught with some substantial difficulties. Moreover, our studies indicate that the reliability on ex situ or indirect methods for characterising particle sizes/dispersions, in this size regime, and as a basis for the subsequent interpretation of kinetic/mechanistic data acquired over a range of temperatures, should not be taken for granted.

Acknowledgements This work was funded by the EPSRC UK (Grant Number GR/60744/01) and the authors thank the EPSRC for the provision of post doctoral and PhD funding to MAN and BJ respectively. The ESRF are thanked for the provision of facilities within a long-term proposal awarded for this research. John James (University of Southampton), and Florian Perrin (ESRF) are gratefully acknowledged for their technical contributions to this work. Dr Gordon McDougall is also greatly thanked for the technical schematics of a novel DRIFTS cell designed and constructed at the department of chemistry, University of Edinburgh, Scotland. MAN would further like to thank the directors of the ESRF for funding for the continued development and implementation of this methodology at the ESRF for the wider use of the scientific community.

References

1. For example, Che M, Bennett CO (1989) Adv Catal 36:55
2. For example, Nieuwenhuys BE (2000) Adv Catal 44:259
3. Granger P, Dujardin C, Paul J-F, Leclercq G (2005) J Mol Cat A 228:241
4. Arai H, Tominaga H (1976) J Catal 43:131–142
5. Liang J, Wang HP, Spicer LD (1985) J Phys Chem 89:5840
6. Srinivas G, Chuang SSC, Debnath S (1994) J Catal 148:748
7. Dictor R (1988) J Catal 109:89
8. Hyde EA, Rudham R, Rochester CH (1988) J Chem Soc Faraday Trans 80:531
9. Anderson JA, Millar GJ, Rochester CH (1990) J Chem Soc Faraday Trans 86:571
10. Root TW, Fisher GB, Schmidt LD (1986) J Chem Phys 85:4679 and ibid (1986) 85:4687
11. Loffreda D, Simon D, Sautet P (1998) Chem Phys Letts 291:15
12. Solymosi F, Bansagi T, Novak E (1988) J Catal 112:183
13. Newton MA, Dent AJ, Diaz-Moreno S, Fiddy SG, Evans J (2002) Angew Chem Intl Ed 41:2587
14. Newton MA, Jyoti B, Dent AJ, Fiddy SG, Evans J (2004) Chem Comm 2382
15. Newton MA, Dent AJ, Fiddy SG, Jyoti B, Evans J (2007) Catal Today, DOI: 10.1016/j.cattod.2006.09.034
16. Newton MA, Fiddy SG, Guilera G, Jyoti B, Evans J (2005) Chem Comm 118
17. Newton MA, Dent AJ, Fiddy SG, Jyoti B, Evans J (2007) Phys Chem Chem Phys 9:246
18. See, for example, (a) Harkness IR, Cavers M, Rees LVC, Davidson JM, McDougall GS (1999) In: Marcus BK, Treacy MMJ, Higgins JB, Bisher ME (eds) Proceedings of the 12th International Zeolite Conference, vol IV. Materials Research Society, Warrendale, PA, p 2615; (b) Cavers M, Davidson JM, Harkness IR, McDougall GS, Rees LVC (1999) In: Froment GF, Waugh KC (eds) Reaction Kinetics and the development of catalytic processes, vol 122. Elsevier, Amsterdam, p 65
19. Binsted N (1988) PAXAS: Programme for the analysis of X-ray adsorption spectra. University of Southampton
20. Binsted N (1998) *EXCURV98*, CCLRC Daresbury Laboratory computer programme
21. Newton MA, Dent AJ, Diaz-Moreno S, Fiddy SG, Jyoti B, Evans J (2006) Chem Eur J 12:1975
22. Clausen BS, Norskov JK (2000) Topics Catal 10:221
23. van Dorssen GE, Koningsberger DC (2003) Phys Chem Chem Phys 5:3549
24. Vant Blik HFJ, Banzon JBAD, Huizinga T, Vis JC, Koningsberger DC, Prins R (1983) J Phys Chem 87:13
25. Suzuki A, Inada Y, Yamaguchi A, Chihara T, Yuasa M, Nomura M, Iwasawa Y (2003) Angew Chem Intl Ed 42:4795
26. Martens JHA, Prins R, Koningsberger DC (1989) J Phys Chem 93:3179
27. Yang AC, Garland CW (1957) J Chem Phys 61:1504
28. (a) Newton MA, Burnaby DG, Dent AJ, Diaz-Moreno S, Evans J, Fiddy SG, Neisius T, Pascarelli S, Turin S (2001) J Phys Chem A 105:5965; (b) Newton MA, Burnaby DG, Dent AJ, Diaz-Moreno S, Evans J, Fiddy SG, Neisius T, Turin S (2002) J Phys Chem B 106:4214
29. Carol LA, Mann GS (1990) Oxid Met 34:1
30. For instance, Salanov AN, Savchenko VI (1994) Kinet Catal 35:722
31. Yao HC, Japar S, Shelef M (1977) J Catal 50:407
32. Vis JC, van't Blik HFJ, Huiizinga T, van Grondelle J, Priins R (1985) J Catal 95:333
33. Chen JG, Colaianni ML, Chen PJ, Yates Jr JT, Fisher GB (1990) J Phys Chem 94:5059
34. Beck DD, Carr CJ (1993) J Catal 144:296
35. Beck DD, Capeheart TW, Wong C, Belton DN (1993) J Catal 144:311
36. Burch R, Lloader PK, Cruise N (1996) Appl Catal A 375
37. Dohmae K, Nonaka T, Seno Y (2005) Surf Interface Anal 37:11
38. Zimowska M, Wagner JB, Dziedzic J, Camra J, Borzecka-Prokop B, Najbar M (2006) Chem Phys Letts 417:137